CHEMISTRY OF MATERIALS

Opening the Hysteresis Loop in MAB Magnets: Experimental and Computational Studies of $CrMn_4SiB_2$ and $Mo_{0.8}Mn_{4.2}SiB_2$

Shola E. Adeniji, Alexei A. Belik, Takao Mori, and Boniface P. T. Fokwa*

Cite This: Chem. Mater. 2025, 37, 2349−2357

Read Online

ACCESS | Metrics & More | Article Recommendations | Supporting Information

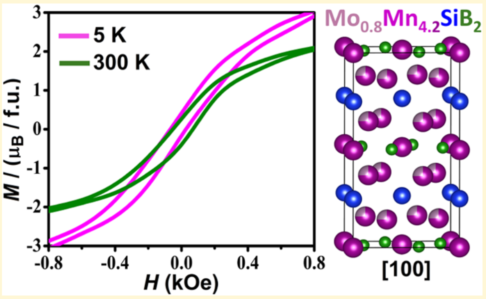

ABSTRACT: This study presents the synthesis and magnetic characterization of two quaternary MAB phases: $CrMn_4SiB_2$ and $Mo_{0.8}Mn_{4.2}SiB_2$. Using a refined synthesis method, we successfully produced single-phase compounds, overcoming previous challenges associated with impurity phases. Both compounds crystallize in the tetragonal space group $I4/mcm$, with Mo demonstrating distinct site preferences in $Mo_{0.8}Mn_{4.2}SiB_2$. Magnetic measurements indicate the presence of long-range ferromagnetic interactions, with Curie temperatures (T_C) of approximately 270 K for $CrMn_4SiB_2$ and 340 K for $Mo_{0.8}Mn_{4.2}SiB_2$. Field-dependent magnetization measurements indicate a saturation magnetization (M_s) of 5.128 μ_B/f.u. (at 5 K) for $CrMn_4SiB_2$ and 6.214 μ_B/f.u. (at 5 K) and 3.692 μ_B/f.u. (at 300 K) for $Mo_{0.8}Mn_{4.2}SiB_2$. The introduction of Mo or Cr in the ternary parent compound Mn_5SiB_2, opens a hysteresis for the first time in this class of T2 phases, with intrinsic coercivities of H_c = 5.57 kA/m for $CrMn_4SiB_2$ and 6.53 kA/m for $Mo_{0.8}Mn_{4.2}SiB_2$. Density functional theory (DFT) calculations confirm the ferromagnetic ordering while the magnetocrystalline anisotropy energy (MAE) calculations show that $CrMn_4SiB_2$ and $MoMn_4SiB_2$ have in-plane anisotropy with higher MAE values than Mn_5SiB_2, thus confirming experimental findings. This research not only introduces a synthesis pathway toward single-phase T2-based quaternary materials, but it also opens an avenue toward MAB-based permanent magnets.

INTRODUCTION

Transition metal borides are increasingly gaining attention for their exceptional properties, which make them attractive for various technological applications.[1−7] Some recent properties of interest concern materials adopting atomically layered structures in which A-group elements like aluminum (Al) or silicon (Si)[8] have been incorporated. The resulting materials can be categorized into various structural families, each demonstrating unique properties. One prominent family of layered materials is the MAX phases, which consist of ternary carbides and nitrides with the general formula $M_{n+1}AX_n$ (where M is a transition metal, A is an A-group element, and X is carbon or nitrogen).[9] These materials combine ceramic and metallic properties, including high thermal stability, mechanical strength, and electrical conductivity. Additionally, selective etching of MAX phases leads to the creation of MXenes, a class of two-dimensional materials with outstanding electrochemical and catalytic properties.[10]

In parallel to MAX phases, another lesser known but structurally related family of materials is the MAB phases. MAB phases are a class of layered transition metal borides characterized by alternating layers of transition metal−boron (MB) and A-site elements. Unlike MAX phases, where the M−X layers (M = transition metal, X = carbon or nitrogen) form strong covalent bonds and are loosely bonded to A elements (enabling their extraction to produce MXenes), MAB phases feature a stronger three-dimensional (3D) bonding network where boron substructures usually exist and are strongly bonded to the A elements (explaining their rather difficult extraction). These boron-based ceramics exhibit various crystal structures, including orthorhombic $M_{n+1}AB_{2n}$ (n = 1−3),[11,12] hexagonal M_2AB_2,[13] and tetragonal M_5AB_2 (T2 phases).[14] Among these MAB phases, the T2 phase Mo_5SiB_2 exhibits relatively isotropic elastic properties, high hardness, enhanced oxidation resistance, fracture toughness, and fatigue-crack resistance.[15,16] Furthermore, $(W,Ta)_5SiB_2$ demonstrates superconducting behavior.[17] Subsequent studies also introduced members of the MAB phase family with interesting magnetic properties, such as Fe_5SiB_2 and Mn_5SiB_2 ferromagnets.[18] First-principles density functional theory (DFT) calculations have reported TM_5SiB_2 (TM = V, Nb, Ta) phases, highlighting their brittleness, anisotropic elastic modulus, and potential as thermal conductor materials.[19]

Recent research has expanded the scope of the T2-MAB phases by synthesizing quaternary compounds incorporating two different transition metals. These quaternary MAB phases

Received: January 24, 2025
Revised: March 3, 2025
Accepted: March 5, 2025
Published: March 12, 2025

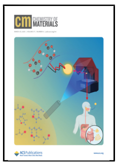

https://doi.org/10.1021/acs.chemmater.5c00187
Chem. Mater. 2025, 37, 2349−2357

either form solid solutions or exhibit chemical ordering, further enhancing their range of properties. For example, Ti_4MoSiB_2 was synthesized as a quaternary solid solution $(Ti_{0.8}Mo_{0.2})_5SiB_2$ exhibiting properties relevant to supercapacitor applications.[20] Meanwhile, the discovery of chemically ordered quaternary MAB phases such as Mo_4MnSiB_2,[21] $Ta_4M''SiB_2$ (M'' = V, Cr, or Mo),[22] and M_4CrSiB_2 (M = Mo, W, Nb),[8] has opened avenues for expanding the chemistry of these materials. These ordered quaternary phases have led to the introduction of the concept of "out-of-plane ordered MAB phases" (o-MAB), where the atomic arrangement is highly ordered. In these o-MAB phases with general formula $M_4M'AB_2$, the larger transition metal (M) tends to occupy the 16l Wyckoff site, while the smaller metal (M') resides in the 4c site. This site preference, driven by the size and electronic configuration of the atoms, plays a crucial role in determining the structural stability of these materials. For instance, in Mo_4MnSiB_2, Mo atoms occupy the 16l sites, while Mn resides in the 4c positions. This specific ordering has been confirmed experimentally[21] and provides insight into the relationship between atomic arrangement and material properties.

Despite significant progress in the synthesis and characterization of MAB phases, achieving single phase quaternary MAB compounds remains complex due to the occasional presence of secondary phases. These secondary phases can obscure a clear understanding of the intrinsic properties of quaternary MAB phases, particularly in relation to their magnetic behavior. For example, studies on quaternary T2-MAB phases, such as Ti_4MoSiB_2,[20] $Ta_4M''SiB_2$ (M'' = V, Cr, or Mo),[22] and M_4CrSiB_2 (M = Mo, W, Nb),[8] have made valuable strides, even as ongoing efforts continue to address the challenges associated with impurity phases. These challenges highlight the need for further refinement in the synthesis process to fully explore their potential for practical applications. In addition, previous computational research efforts have demonstrated that elemental substitution can improve the magnetic properties of these compounds. For instance, investigations by Wenwinski et al. suggested incorporating Co into Fe_5SiB_2 could enhance the magnetocrystalline anisotropy energy (MAE).[23] Likewise, Wenwinski et al. found that doping Fe_5PB_2 with 5d elements such as W or Re doubled the MAE.[24] Lastly, Thakur et al. showed that Cr substitution in Fe_5SiB_2 not only enhances the MAE but it also changes its sign due to spin−orbit interactions,[25] This proposed improvement of MAE stands in contrast to the soft magnetic behavior observed experimentally in $Fe_5Si_{1-x}Ge_xB_2$,[26] where no magnetic hysteresis was found after Ge substitution, although in this work only the nonmagnetic element (Si) was substituted. While Mn_5SiB_2[12] is a soft ferromagnet, the o-MAB Mo_4MnSiB_2 is paramagnetic,[21] suggesting that too many Mo atoms destroy the long-range magnetic order in Mn_5SiB_2, thus, to obtain quaternary phases showing magnetic ordering, Mn-rich phases must be targeted. Our research aimed at addressing these challenges by introducing two quaternary Mn-rich MAB phases, $CrMn_4SiB_2$ and $Mo_{0.8}Mn_{4.2}SiB_2$, obtained by substitution of the magnetic element (Mn) by Cr and Mo in the soft ferromagnet Mn_4SiB_2. Alongside experiments, density functional theory (DFT) calculations were employed to understand the stability, electronic and magnetic properties of $CrMn_4SiB_2$ and $Mo_{0.8}Mn_{4.2}SiB_2$ (modeled by ideal $MoMn_4SiB_2$). We demonstrate that these are the first T2-type MAB phases showing significant opening of hysteresis with coercivities.

■ MATERIALS AND EXPERIMENTAL PROCEDURES

Synthesis. The compounds $CrMn_4SiB_2$ and $Mo_{0.8}Mn_{4.2}SiB_2$ were synthesized from elemental powders of Molybdenum (Mo, 99.9%, Thermo Scientific), chromium (Cr, 99.5%, Alfa Aesar), manganese (Mn, 99% Aldrich), silicon (Si, 99.5%, Alfa Aesar), and boron (B, 97%, amorphous powder, Thermo Scientific). The elements were weighed to achieve the correct stoichiometric ratios with a total mass of 200 mg for each batch. A synthesis using the ideal composition $MoMn_4SiB_2$ was also tried but it led to the formation of a side phase, suggesting that the ideal composition may not form using this synthesis procedure.

The weighed elements were thoroughly ground together, and the resulting mixtures were compacted into pellets using a hydraulic press. These pellets were placed into dried and evacuated quartz ampules, which were then sealed under an argon atmosphere to prevent oxidation. The standard heating profile used to prepare MAB phases was not successful in preparing single phases, so we tried a different approach. The box furnace was preheated to 1220 °C within 1 h before inserting the samples. The furnace temperature was maintained for 18 h, then the ampules were removed and quenched in cold water to rapidly cool the samples. This process resulted in a homogeneous mixture of spherical gray, metallic products for both $CrMn_4SiB_2$ and $Mo_{0.8}Mn_{4.2}SiB_2$.

Powder X-ray Diffraction (PXRD) and Rietveld Refinement. The synthesized metallic products were first manually crushed and finely ground using an agate mortar and pestle to ensure homogeneity for further analysis. Powder X-ray diffraction (PXRD) analysis was employed to identify the phase purity and structural details of the synthesized samples. The diffraction data were initially collected using a Rigaku Miniflex 600 diffractometer, which operates with Cu−Kα_1 radiation (λ = 1.540593 Å). A Dectris MYTHEN2 1K detector was utilized for optimal signal detection. The diffraction data were recorded in a continuous scan mode over the 2θ range of 5−90°, with a step size of 0.015°. Each scan was conducted over a duration of 4 h to ensure adequate signal-to-noise ratios and minimize the influence of background noise.

Rietveld refinement was carried out using established methods,[27] for the determination of lattice parameters, crystal structure and provided insights into the phase composition and crystallinity of the synthesized materials.

Energy Dispersive X-ray (EDX) Spectroscopy. The microstructures and chemical compositions of $CrMn_4SiB_2$ and $Mo_{0.8}Mn_{4.2}SiB_2$ were analyzed using EDX spectroscopy on a Tescan Vega3 SBH scanning electron microscope (SEM), equipped with a Bruker L-N_2-free high-resolution 30 mm^2 SD detector. The detector's energy resolution was ≤129 eV at Mn Kα, and it was calibrated with reference materials to ensure accuracy. The detection range covered elements from boron to californium, allowing a comprehensive analysis of light and heavy elements. Multiple regions of each sample were examined to assess homogeneity, and quantitative data were corrected using ZAF procedures. Backscattered electron imaging was also employed to correlate microstructure with elemental composition. The measurements were conducted at 20 kV with a 15 mm working distance under high vacuum.

Magnetization Measurements. The magnetic properties of $CrMn_4SiB_2$ and $Mo_{0.8}Mn_{4.2}SiB_2$ were studied using a Quantum Design MPMS3 SQUID magnetometer. Magnetic susceptibility measurements were performed between 2 and 400 K (at H = 0.01 T) in both zero-field-cooled (ZFC) and field-cooled (FC) conditions, while field-dependent magnetization curves were recorded at various temperatures to assess hysteresis and saturation. To get more reliable Curie−Weiss fits magnetic data were collected at H = 1 T under DC mode. The inverse susceptibility curves were fitted between 340 and 400 K for $CrMn_4SiB_2$ and between 375 and 400 K for $Mo_{0.8}Mn_{4.2}SiB_2$.

Computational Methods. To investigate the electronic and magnetic properties of the quaternary compounds $CrMn_4SiB_2$ and

$Mo_{0.8}Mn_{4.2}SiB_2$, density functional theory (DFT) calculations were all performed utilizing the Vienna Ab Initio Simulation Package (VASP).[28,29] The generalized gradient approximation (GGA) was employed with the Perdew−Burke−Ernzerhof (PBE) functional to describe the exchange and correlation effects.[30−32]

For the study of $Mo_{0.8}Mn_{4.2}SiB_2$, the ideal composition $MoMn_4SiB_2$ was used. Given that a Mn-site preference as well as site-sharing between Mo and Mn was found experimentally (see below) two structure models (Mo in the 4c and Mo in the 16l sites) were evaluated to ascertain the most probable distribution of Mo and Mn within the unit cell. Each model's initial structure underwent optimization, allowing the lattice parameters, cell shape, volume, and atomic positions to fully relax. The projector augmented wave (PAW) method was utilized to accurately treat core electrons. For Brillouin zone sampling, a Monkhorst−Pack[32] *k*-point mesh of 6 × 6 × 3 was used. The plane wave cutoff energy was set to 550 eV, providing sufficient basis set quality for the calculations. A rigorous convergence criterion of 10^{-6} eV per cell was established for total energy calculations, ensuring precision in the energy landscape analysis. Following structural relaxation, self-consistent (SC) calculations were performed to confirm electronic convergence. The most energetically favorable structure was identified based on final total energy calculations. After structure optimization, we performed Density of States (DOS) calculations using the charge density data obtained from the CHGCAR file generated during the self-consistent (SC) calculations. The DOS was evaluated on a grid of 2000 points (NEDOS) to ensure adequate resolution of the electronic states. For visualization purposes the Fermi energy (E_F) was normalized to 0 eV. Magnetic ordering was probed by nonspin polarized and spin polarized calculations using the relaxed structures.

Spin−orbit coupling (SOC) calculations were performed using eq 1 to evaluate the magnetocrystalline anisotropy energy (MAE). MAE represents the energy difference between two magnetic orientations along different crystallographic axes, such as the *a*-axis and *c*-axis. This anisotropy is a result of SOC and the crystal lattice's symmetry, which determines the preferred direction for spin alignment. The expression for SOC is given in eq 1, and MAE is calculated using eq 2

$$H_{SOC} = \xi \mathbf{L} \cdot \mathbf{S} \tag{1}$$

$$\mathrm{MAE} = E_{SOC}(\parallel c) - E_{SOC}(\perp c) \tag{2}$$

Here, H_{SOC} represents the spin−orbit coupling Hamiltonian, where ξ is the SOC constant, $\mathbf{L}$ is the orbital angular momentum, and $\mathbf{S}$ is the spin angular momentum. $E_{SOC}(\| c)$ is the total energy when the magnetization is aligned along the *c*-axis. $E_{SOC}(\perp c)$ is the total energy when the magnetization is aligned along the *a*-axis (or perpendicular to *c*-axis). The MAE quantifies the energy difference between spins aligned parallel and perpendicular to the *c*-axis.

RESULTS AND DISCUSSION

Synthesis, Crystal Structure, and Site Preference. These two targeted compounds were synthesized using a box furnace with carefully controlled stoichiometric ratios of the constituent elements. Powder X-ray diffraction (PXRD) analysis was conducted to confirm the purity and crystalline structure of each sample. As illustrated in Figure 11(a,b) both $CrMn_4SiB_2$ and $Mo_{0.8}Mn_{4.2}SiB_2$ were achieved as crystalline single phases according to PXRD. In contrast, a similar synthesis using the ideal $MoMn_4SiB_2$ starting composition exhibited an 18% Mo_2MnB_2 impurity (see Figure S1), thus suggesting that substituting more than 80% Mn by Mo in Mn_5SiB_2 structure leads to the formation of a competing Mo-richer phase thereby preventing single-phase synthesis. However, Tao et al.[21] showed recently that the highly Mo-rich phase Mo_4MnSiB_2 can be synthesized as a crystalline single-phase material, but this is rather an exception in the family of o-MAB phases, given that all other reported cases did not produce single-phase products, to the best of our knowledge.[5,13−15] Indeed, our attempt to synthesize these phases using the reported synthesis conditions (ramping the furnace with samples to 1500 °C, then quenching) for other quaternary o-MAB phases failed, as the product contained mainly Mn_5Si_3 and Mn_3B_4 phases at this temperature.

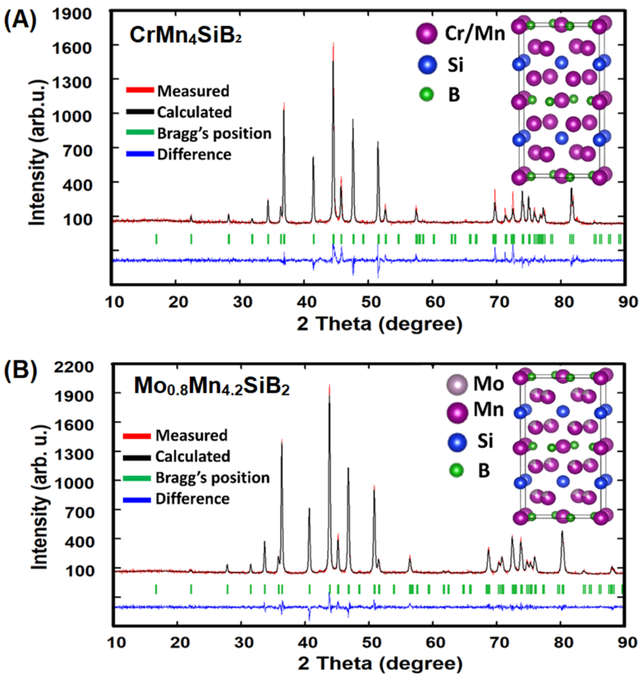

Figure 1. Rietveld refinement plots of the powder XRD data (collected using Mo radiation) for $CrMn_4SiB_2$ (A) and $Mo_{0.8}Mn_{4.2}SiB_2$ (B). Insets are their respective refined unit cells.

Indexing the X-ray diffractograms confirmed that both $CrMn_4SiB_2$ and $Mo_{0.8}Mn_{4.2}SiB_2$ are isostructural, crystallizing in the tetragonal T2-type structure (space group *I*4/*mcm*, #140) also adopted by the parent Mn_5SiB_2 phase. The refined unit cell parameters (see Table 1) of both phases are, respectively, slightly smaller and larger than those of the ternary Mn_5SiB_2 phase (a = 5.608 Å and c = 10.432 Å),[12] which is expected given the gradual increase in atomic radii of

Table 1. Results of Rietveld Refinement for $CrMn_4SiB_2$ and $Mo_{0.8}Mn_{4.2}SiB_2$ Based on XRD Data from Figure 1(a,b)

		$CrMn_4SiB_2$	$Mo_{0.8}Mn_{4.2}SiB_2$
unit cell parameter	space group	*I*4/*mcm*, 140	*I*4/*mcm*, 140
	a = b (Å)	5.6064(2)	5.6777(2)
	c (Å)	10.4244(2)	10.6403(4)
	$\alpha = \beta = \gamma$	90.0°	90.0°
	V ($Å^3$)	327.66(3)	343.01(3)
	density (g/cm^3)	6.517	6.918
Wyckoff site	4c	Mn, Cr: 0, 0, 0	Mn: 0, 0, 0
	16l	Mn, Cr: 0.1693(3), 0.6693(3), 0.1393(0)	80% Mn, 20% Mo: 0.1689(2), 0.6689(2), 0.1390(2)
	4a	Si: 0, 0, 0.25	Si: 0, 0, 0.25
	8h	B: 0.385(3), 0.885(3), 0	B: 0.384(2), 0.884(2), 0
rietveld refinement	R_{Bragg}	7.32	4.23
	R_f	7.51	4.15
	χ^2	1.87	1.32

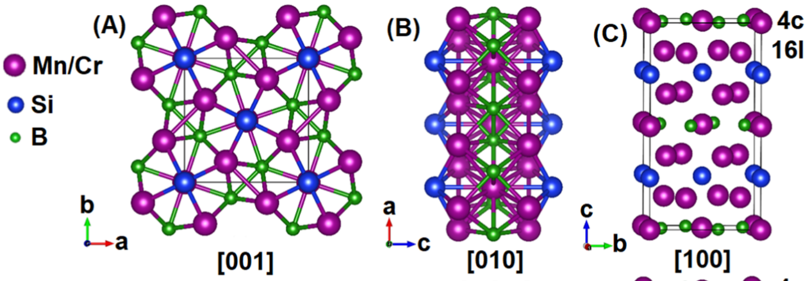

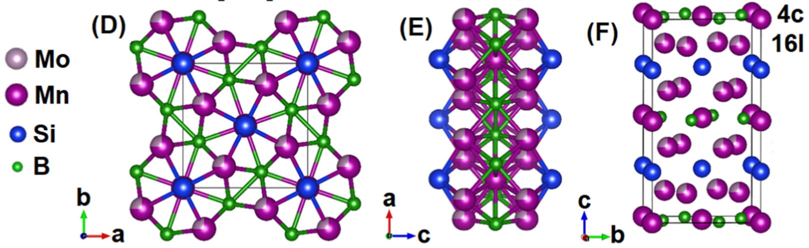

Figure 2. Structure models of the T2 phases $CrMn_4SiB_2$ (A−C) and $Mo_{0.8}Mn_{4.2}SiB_2$ (D−F) viewed along the [001], [010], and [100] crystallographic directions.

the key elements Cr, Mn and Mo in this order. Similarly, increasing the molybdenum content should lead to increase unit cell parameters, as observed indeed for Mo_4MnSiB_2 (a = 5.938 Å, c = 11.057 Å).[14] Rietveld refinements were carried out for both PXRD data using Mn_5SiB_2 structure as the starting structure model, then two models were derived; one statistical (Mo/Mn mixed on the 2 Mn sites) and a site-preferential model (Mn alone on 4c) according to the ordered o-MAB phase Mo_4MnSiB_2. For the $CrMn_4SiB_2$ phase, the outcome of Rietveld refinement did not reveal any specific site preference for the constituent elements. This is expected, given the difficulty in distinguishing between Cr and Mn atoms by X-ray diffraction, as both differ by only one electron. However, the ordered model cannot be entirely excluded because an electronic argument is found to be more viable than an atomic size argument for the Mo-based phase (see below). Also, DFT calculations slightly favor Cr on 16l (see below). Figure 2(a−c) display several projections of the $CrMn_4SiB_2$ unit cell along the [001], [010], and [100] crystallographic directions.

The refinement of the Mo-based diffractogram clearly favors the ordered o-MAB $Mo_{0.8}Mn_{4.2}SiB_2$ model with only Mn found on the 4c Wyckoff site, while both Mo and Mn share the 16l site (Figure 3). This site-specific occupancy is supported by electronic arguments rather than atomic size ones, wherein the valence electron (VE) richer but smaller element (Mn with 7 VE) preferentially occupies the larger 4c site over the VE-poorer and larger element (Mo with 6 VE) as shown in Figure 3.

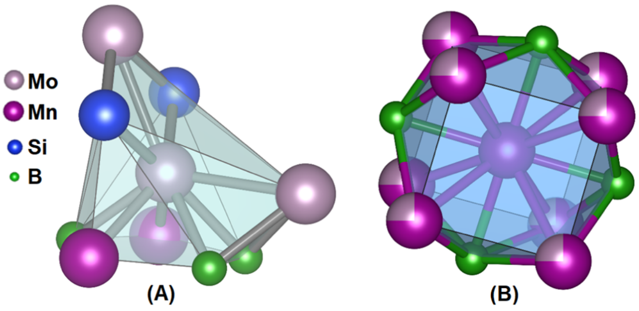

Figure 3. Distorted pentagonal prism around Mo (A) and cuboctahedron around Mn (B).

The higher VE number of Mn facilitates the building of a larger coordination sphere with neighboring atoms, leading to a more stable structure overall. This preference for specific atomic positions is shown in Figure 2(d−f) along different crystallographic directions ([001], [010], and [100]). The quaternary out-of-plane ordered MAB (o-MAB) phases, such as $Mo_{0.8}Mn_{4.2}SiB_2$, build upon the notable chemical ordering which occurs when the elements M and M′ selectively occupy the 16l and 4c sites, respectively, in the general composition $M_4M'SiB_2$ (M = Mo, W, Nb, Ta M′ = Cr, Mn). 5,13−15

SEM-EDS Analysis for Elemental Distribution in Microstructures. The elemental distribution maps, shown in Figure 4, reveal homogeneous distribution throughout the samples. Using energy dispersive X-ray spectroscopy (EDS) the elemental ratios of the heavy elements (Mo, Cr, and Si) were measured (Table 2), leading to the estimated compositions that align closely with the expected starting compositions, the largest discrepancy being an 8.5% deviation for Mn in $Mo_{0.8}Mn_{4.2}SiB_2$. The compositional errors observed fall within the standard error range of the EDS quantification, ensuring the accuracy and reliability of the data. This confirms that the samples are generally phase-pure with a homogeneous distribution of elements. The EDS spectra, which include the peaks and the percentage composition of each element, are provided in the Supporting Information (Figure S2).

Experimental Magnetism. Magnetic measurements were performed on the $CrMn_4SiB_2$ and $Mo_{0.8}Mn_{4.2}SiB_2$ compounds, with temperature-dependent magnetization (M−T) curves [Figure 5(a,b)] measured at 0.01 T (100 Oe) under zero-field cooled (ZFC) and field-cooled (FC) conditions. Magnetic susceptibility measurements showed similar magnetic behaviors for the two phases. A ferromagnetic to paramagnetic phase transition is observed near room temperature, with Curie temperatures (T_C) of approximately 270 K for $CrMn_4SiB_2$ and 340 K for $Mo_{0.8}Mn_{4.2}SiB_2$.

These T_C values are lower than even the smallest value reported for the ternary parent compound Mn_5SiB_2 (406,[3] 411,[33] 441,[34] and 470 K).[35] In fact, in $Mo_{0.8}Mn_{4.2}SiB_2$, a 16% Mo substitution lowers T_C by approximately 100 K, while a

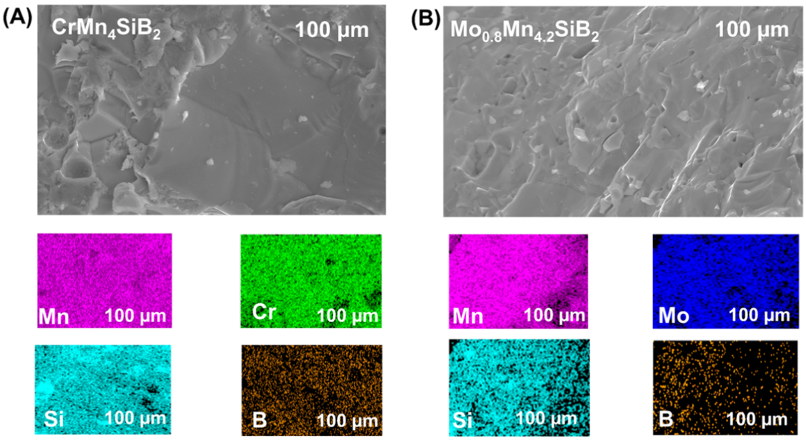

Figure 4. Results of the SEM−EDS analysis. Panel (A) displays the SEM image of $CrMn_4SiB_2$, while panel (B) shows the SEM image of $Mo_{0.8}Mn_{4.2}SiB_2$. Below each image, EDS maps for all elements are provided.

Table 2. Elemental Composition and Homogeneity Assessment of $CrMn_4SiB_2$ and $Mo_{0.8}Mn_{4.2}SiB_2$ Phases

sample	element content	% loaded	% measured
$CrMn_4SiB_2$	Mn	66.7	64.8
	Cr	16.7	17.6
	Si	16.7	17.6
$Mo_{0.8}MnSiB_2$	Mn	70.0	76.2
	Mo	16.7	13.0
	Si	13.3	10.7

more pronounced decrease (by about 200 K) is seen with a 20% Cr substitution. This decrease in T_C is not surprising for $Mo_{0.8}Mn_{4.2}SiB_2$, given that a nonmagnetic element (Mo) is substituting for a magnetic one (Mn) in the Mn_5SiB_2 parent compound. For $CrMn_4SiB_2$, both Cr and Mn are magnetic elements, thus the reason for the decrease in T_C is not as obvious and will be discussed below in the DFT section. The inverse susceptibility curves for $CrMn_4SiB_2$ and $Mo_{0.8}Mn_{4.2}SiB_2$, displayed in Figure 5(c,d), reveal positive Weiss constants of $\theta = 289$ K and $\theta = 351$ K, respectively. These values, derived from the application of the Curie−Weiss law, further support the presence of strong ferromagnetic interactions. Also, they are close to the respective Curie temperatures ($T_C = 270$ K for $CrMn_4SiB_2$ and $T_C = 340$ K for $Mo_{0.8}Mn_{4.2}SiB_2$), suggesting the absence of spin frustration in these systems.

Figure 6(a,b) display the field-dependent magnetization ($M-H$) curves for $CrMn_4SiB_2$ and $Mo_{0.8}Mn_{4.2}SiB_2$, measured at 5, 200, and 300 K, and the derived magnetic parameters are summarized in Table 3. At 5 K, the saturation magnetization (M_s) of $CrMn_4SiB_2$ and $Mo_{0.8}Mn_{4.2}SiB_2$ under an applied field of 70 kOe (7 T) reaches 5.13 μ_B/f.u. and 6.21 μ_B/f.u., respectively. At higher temperatures, M_s decreases to 3.48 μ_B/

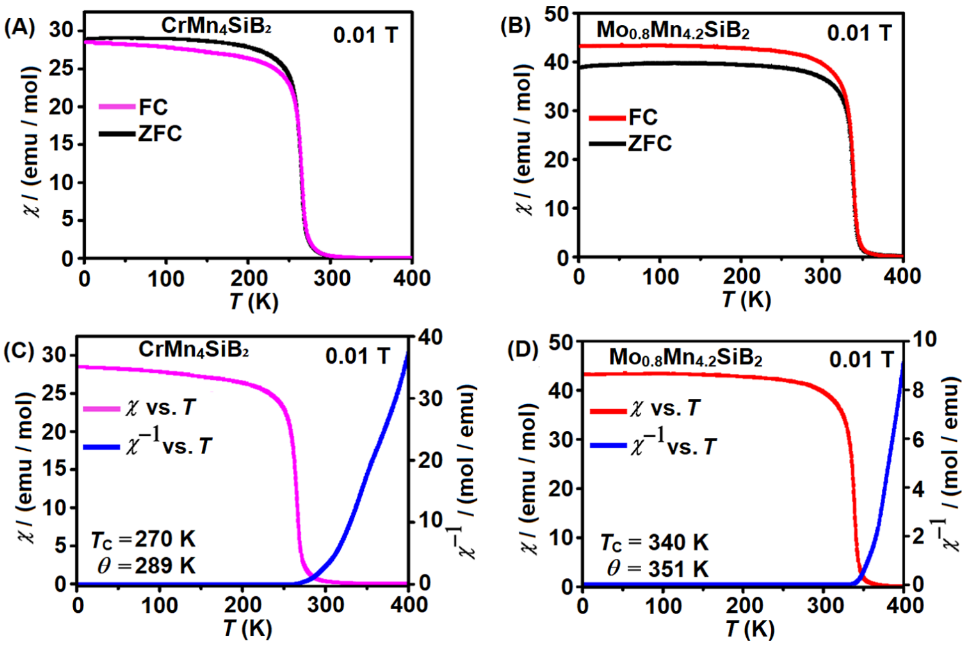

Figure 5. Panels (A, B) present the magnetic susceptibility as a function of temperature measured at 0.01 T in both zero-field-cooled (ZFC) and field-cooled (FC) conditions. Panels (C, D) illustrate the temperature dependence of the magnetic susceptibility, along with its inverse, also measured at 0.01 T.

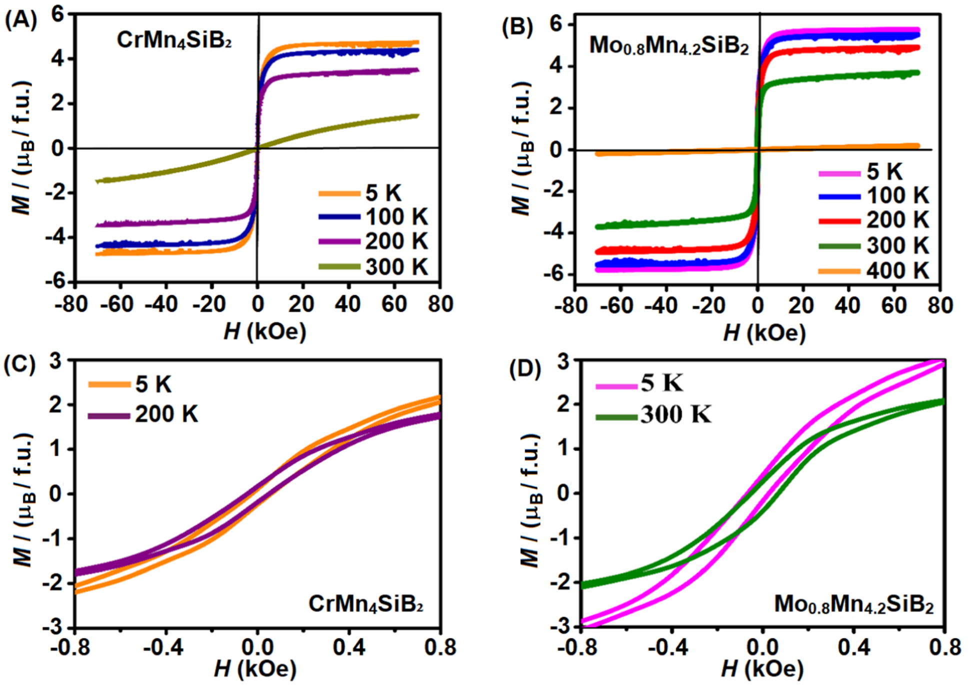

Figure 6. Magnetization versus magnetic field (M−H) data for $CrMn_4SiB_2$ and $Mo_{0.8}Mn_{4.2}SiB_2$ across various temperatures. Panels (A, B) display (M−H) curves measured at 5, 100, 200, 300 and 400 K, showing their temperature dependence. Panel (C) focuses on the hysteresis loops measured at 5 and 200 K for $CrMn_4SiB_2$, highlighting the evolution of coercivity and remanence with temperature. Panel (D) shows the hysteresis loops measured at 5 and 300 K for $Mo_{0.8}Mn_{4.2}SiB_2$.

Table 3. Summary of Curie Temperature (T_C), Curie−Weiss Constant (θ), and Saturation Magnetization (M_s) for the Discovered Quaternary Phases

magnetic parameters	$CrMn_4SiB_2$	$Mo_{0.8}Mn_{4.2}SiB_2$
T_C	270 K	340 K
θ	289 K	351 K
M_s at 5 K (70k Oe)	5.128 μ_B/f.u (1.282 μ_B/Mn)	6.214 μ_B/f.u (1.554 μ_B/Mn)
M_s at 100 K (70k Oe)	4.386 μ_B/f.u (1.092 μ_B/Mn)	5.520 μ_B/f.u (1.314 μ_B/Mn)
M_s at 200 K (70k Oe)	3.481 μ_B/f.u (0.870 μ_B/Mn)	4.901 μ_B/f.u (1.167 μ_B/Mn)
M_s at 300 K (70k Oe)	1.472 μ_B/f.u (0.368 μ_B/Mn)	3.692 μ_B/f.u (0.879 μ_B/Mn)

f.u. (at 200 K) for $CrMn_4SiB_2$ and 3.69 μ_B/f.u. (at 300 K) for $Mo_{0.8}Mn_{4.2}SiB_2$. From the results presented in Table 3, the average magnetic moment per manganese atom at 5 K is 1.18 μ_B/Mn for $CrMn_4SiB_2$ and 1.36 μ_B/Mn for $Mo_{0.8}Mn_{4.2}SiB_2$. As the temperature increases , these values drop to 0.87 μ_B/Mn (at 200 K) and 0.88 μ_B/Mn (ar 300 K), respectively. This decline in magnetization with increasing temperature is consistent with typical magnetic behavior as thermal energy disrupts alignment of magnetic centers. These results are comparable to previously reported data. For instance, Wäppling et al. reported an average magnetic moment of 1.6 μ_B/Mn for the ternary parent compound Mn_5SiB_2,[33] while de Almeida et al. observed a magnetic moment of 0.946 μ_B/Mn at 300 K for the same compound.[35]

More recently, Ojiyed et al.[36] reported magnetic moments for Mn_5SiB_2 of 1.37 μ_B/Mn and 0.88 μ_B/Mn at 5 and 300 K, respectively.

In Figure 6c, the hysteresis loop for $CrMn_4SiB_2$ shows coercivity values of 0.07 kOe (H_c = 5.57 kA/m) at 5 K and 0.06 kOe (H_c = 4.77 kA/m) at 200 K. Notably, no magnetic hysteresis loop is observed at 300 K, confirming its below room temperature ordering (T_C = 270 K). In Figure 6d, the hysteresis loop for $Mo_{0.8}Mn_{4.2}SiB_2$ shows coercivity values of 0.082 kOe (H_c = 6.53 kA/m) at 5 K and 0.065 kOe (H_c = 5.17 kA/m) at 300 K. However, these coercivity values lie closer to the soft magnetic range (H_c < 1 kA/m) than the hard magnetic range (H_c > 30 kA/m). Nevertheless, this is a significant discovery because it represents the first reported hysteresis opening observed for T2 phases, to the best of our knowledge. For comparison, the ternary parent compound Mn_5SiB_2 has been reported to exhibit typical soft ferromagnetic behavior, characterized by the absence of magnetic hysteresis.[36] Although Elmeligy et al. observed a small hysteresis loop they reported negligible coercivity.[34] For similar MAB phases, Clulow et al. reported near-zero coercivity and magnetic remanence at 10 and 300 K for $Fe_5Si_{1-x}Ge_xB_2$.[26] However, computational works have suggested a possible realization of hard magnetic T2-MAB phases. For instance, some investigations suggested incorporating Co or Cr into Fe_5SiB_2 to enhance the magnetocrystalline anisotropy energy (MAE)[23] or the finding that doping Fe_5PB_2 with 5d elements such as W or Re doubled its MAE.[24]

Computational Results and Discussion. We carried out computational analysis to verify the experimentally found site preference, magnetic ordering and understand the origin of enhanced coercivities in these two compounds. For computational analysis of $Mo_{0.8}Mn_{4.2}SiB_2$ the ideal composition $MoMn_4SiB_2$ was modeled. Relaxation energy calculations were performed for both $CrMn_4SiB_2$ and $MoMn_4SiB_2$ structures using nonspin polarized (nsp) and spin polarized (sp) models. The results showed that the sp calculations for both compounds were more stable compared to their nsp counterparts, indicating the likelihood of magnetic ordering in these structures, as found experimentally. Specifically, the

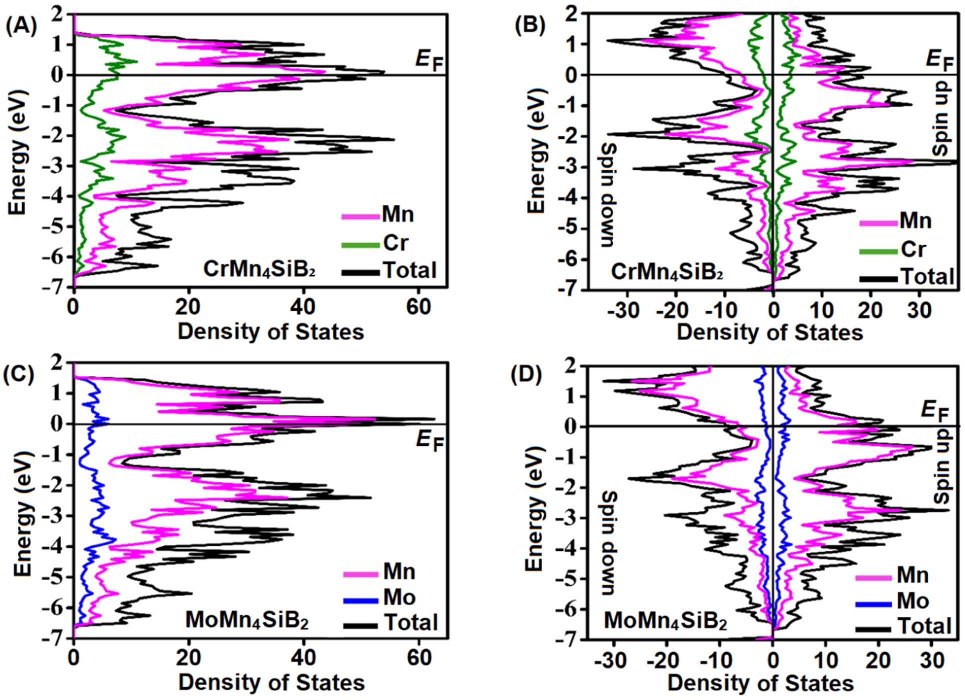

Figure 7. Total and partial density of states (DOS) for $CrMn_4SiB_2$ and $MoMn_4SiB_2$ in both nonspin-polarized and spin-polarized configurations. Panels (A, B) show the DOS for $CrMn_4SiB_2$ without and with spin polarization, respectively, while panels (C, D) show the corresponding DOS plots for $MoMn_4SiB_2$ under the same conditions.

energy difference between the nsp and sp models for $CrMn_4SiB_2$ was found to be +1.760 eV, while for $MoMn_4SiB_2$, it was slightly higher at +1.884 eV. The density of states (DOS) plots, illustrated in Figure 7(a−d), provide additional insight into the magnetic properties of these structures. The calculated DOS indicates that the magnetism in both $CrMn_4SiB_2$ and $MoMn_4SiB_2$ is predominantly contributed by the d orbitals of Mn. In the nsp DOS, significant states are present near the Fermi level (E_F) for both structures, indicating metallic behavior. The sp DOS shows substantial exchange splitting of 2 to 3 eV, with Mn states dominating the electronic structure around E_F. In particular, the sp DOS of $MoMn_4SiB_2$ exhibits more pronounced spin splitting of the Mn states compared to $CrMn_4SiB_2$, suggesting larger magnetic moments. However, the calculated total magnetic moment for $MoMn_4SiB_2$ is 6.47 μ_B/f.u., which is only marginally greater than the 6.36 μ_B/f.u. calculated for $CrMn_4SiB_2$. This difference suggests that the $MoMn_4SiB_2$ structure exhibits only slightly greater ferromagnetic interactions if compared to the $CrMn_4SiB_2$ structure, which is surprising given that the experimental $MoMn_4SiB_2$ phase has a much larger magnetic moment (6.21 μ_B/f.u.) if compared to the 5.13 μ_B/f.u. found for $CrMn_4SiB_2$. The difference between the computational and experimental values for the Mo-based phase can be explained by the larger amount of Mn in the experimental composition ($Mo_{0.8}Mn_{4.2}SiB_2$). However, the much larger difference between the computational and experimental values found for the Cr-based phase is unusual. In fact, the calculated elemental average magnetic moment in $CrMn_4SiB_2$ are 1.27 μ_B/Mn, and 0.44 μ_B/Cr with small negative contributions from B (∼−0.11 μ_B) and Si (∼−0.077 μ_B). Not accounting for the Cr moment leads to an average moment of 5.08 μ_B which is much closer to the experimental value, suggesting an overestimation of the Cr moment by DFT. Indeed, the calculated total magnetic moment of $MoMn_4SiB_2$ is closer to the experimental value because the elemental moment of Mo is negligible (∼0.01 μ_B). In both compounds, the Mn at the 16l site possesses a larger magnetic moment than at the 4c site. The calculated magnetic moment of 1.30 μ_B/Mn from DFT closely matches the experimental value of 1.36 μ_B/Mn measured at 5 K for $Mo_{0.8}Mn_{4.2}SiB_2$ (as shown in Table 3). For comparison, the ternary parent compound Mn_5SiB_2 has a DFT-calculated average magnetic moment of 1.57 μ_B per Mn atom, with 1.7 μ_B at the 16l site and 1.3 μ_B at the 4c site.[34] Although de Almeida et al. reported a slightly lower value of 1.5−1.6 μ_B per Mn atom,[35] they speculated that this discrepancy might be due to ferrimagnetic ordering. Elmeligy et al. later tested this hypothesis, concluding that the ferrimagnetic state, with minority Mn atoms having opposite spin, results in a higher energy state and a net moment of only 0.78 μ_B per Mn atom, which does not align with experimental results. In this study, our sp calculations on Mn_5SiB_2 confirm an average magnetic moment of 1.56 μ_B per Mn atom, closely matching the reported values.[29,35] These results strongly support the conclusion that the magnetic ground state of Mn_5SiB_2 as well as the here reported quaternaries is FM, with site-dependent variations in the Mn magnetic moments.

To understand the opening of hysteresis found for $CrMn_4SiB_2$ and $Mo_{0.8}Mn_{4.2}SiB_2$, magnetocrystalline anisotropic energy (MAE) calculations were performed. The calculated MAE values are positive (+0.202 and +0.224 meV/f.u. for $CrMn_4SiB_2$ and $MoMn_4SiB_2$, respectively) indicating a preference for spin orientation perpendicular to the *c*-axis (easy plane behavior). The positive MAE values are indicative of weak overall anisotropy for both phases, with slightly greater anisotropy for the Mo-based phase. These results confirm experimental findings of small coercivity values for both phases. Also, the experimentally found larger coercivity for $Mo_{0.8}Mn_{4.2}SiB_2$ is confirmed by these DFT results. In comparison, our DFT results for the ternary parent compound Mn_5SiB_2 also show a positive but smaller MAE of +0.180 meV/f.u., which is indicative of a smaller anisotropy than the quaternary compounds, supporting experimental findings. For comparison, Thakur et al. computationally investigated Cr substitution at the Fe 4c site in Fe_5SiB_2.[25] They found that Cr reverses the MAE, changing its sign, despite suppressing the magnetic moment of nearby Fe atoms. This shift in MAE was attributed to changes in the local electronic environment induced by SOC. Similarly, Werwinski et al. demonstrated that alloying Fe_5SiB_2 with Co[23] or doping Fe_5PB_2 with 5d elements like W or Re[24] significantly increase the MAE. In our study, substituting Cr into the Mn_5SiB_2 structure did not change the sign of MAE as was reported for Cr substitution in Fe_5SiB_2,[25] however it enhances MAE just like in the case of Co alloying.[23] The contrasting results found in these DFT calculations are likely because different structure models were used for those calculations: While the Cr substitution in Fe_5PB_2 assumed a site preference (Cr only in the 4c site) the Co substitution was made on the two available sites (alloying). In our calculations of $MoMn_4SiB_2$, we assigned Mo on the 16l site as found experimentally and it resulted in enhanced MAE value if compared to Mn_5SiB_2 but without changing of orientation, in accordance with W and Re substitution[24] in Fe_5PB_2. The enhanced MAE in these quaternary compounds suggests the possibility of achieving semihard to hard magnetic behaviors in T2 phases in the future.

CONCLUSIONS

This study presents the successful synthesis and comprehensive magnetic analysis of two quaternary T2-MAB phases, $CrMn_4SiB_2$ and $Mo_{0.8}Mn_{4.2}SiB_2$. The modified synthesis approach resulted in single-phase products. Powder X-ray diffraction (PXRD) confirmed the phase purity and crystallinity of these materials, revealing that both compounds crystallize in the tetragonal space group $I4/mcm$. Magnetic measurements indicate that both $CrMn_4SiB_2$ and $Mo_{0.8}Mn_{4.2}SiB_2$ exhibit ferromagnetic behavior, with Curie temperatures (T_C) of 270 and 340 K, respectively. Field-dependent magnetization measurements reveal saturation magnetization values of 5.13 μ_B/f.u. for $CrMn_4SiB_2$ and 6.21 μ_B/f.u. for $Mo_{0.8}Mn_{4.2}SiB_2$ at 5 K. For the first time, the opening of magnetic hysteresis is found in T2 phases, as both phases show significant coercivities. DFT calculations confirmed the structural stability and the ferromagnetic ordering for both phases, while also suggesting larger MAE values for these phases if compared to the known soft Mn_5SiB_2 ferromagnet, confirming experimental findings. Future works could further investigate the role of heavier transition metal on the structural and magnetic characteristics of these materials, with potential to discover semihard and hard magnets.

ASSOCIATED CONTENT

Supporting Information

The Supporting Information is available free of charge at https://pubs.acs.org/doi/10.1021/acs.chemmater.5c00187.

> Rietveld refinement plot of the powder XRD data; SEM images and EDS spectra of the reported compounds (PDF)

AUTHOR INFORMATION

Corresponding Author

Boniface P. T. Fokwa − *Department of Chemistry, University of California, Riverside, California 92521, United States;* orcid.org/0000-0001-9802-7815; Email: bfokwa@ucr.edu; www:fokwalab.ucr.edu

Authors

Shola E. Adeniji − *Department of Chemistry, University of California, Riverside, California 92521, United States*
Alexei A. Belik − *Research Center for Materials Nanoarchitectonics (MANA), National Institute for Materials Science (NIMS), Tsukuba 305-0044, Japan;* orcid.org/0000-0001-9031-2355
Takao Mori − *Research Center for Materials Nanoarchitectonics (MANA), National Institute for Materials Science (NIMS), Tsukuba 305-0044, Japan; Graduate School of Pure and Applied Sciences, University of Tsukuba, Tsukuba 305-8577, Japan;* orcid.org/0000-0003-2682-1846

Complete contact information is available at: https://pubs.acs.org/10.1021/acs.chemmater.5c00187

Notes

The authors declare no competing financial interest.

ACKNOWLEDGMENTS

B.P.T.F. acknowledges financial support from UC Riverside (CoR seed grant). T.M. acknowledges support from JST Mirai Program (JPMJMI19A1). We are grateful to the advanced computing and data resource program (ACCESS, funded by NSF) for allocations provided to support our DFT calculations at the San Diego Supercomputing Center.

DEDICATION

In Memory of Prof. Francis J. DiSalvo.

REFERENCES

(1) Kawashima, K.; Márquez, R. A.; Smith, L. A.; Vaidyula, R. R.; Carrasco-Jaim, O. A.; Wang, Z.; Son, Y. J.; Cao, C. L.; Mullins, C. B. A Review of Transition Metal Boride, Carbide, Pnictide, and Chalcogenide Water Oxidation Electrocatalysts. *Chem. Rev.* **2023**, *123*, 12795−13208.

(2) Albert, B.; Hillebrecht, H. Boron: Elementary Challenge for Experimenters and Theoreticians. *Angew. Chem., Int. Ed.* **2009**, *48*, 8640−8668.

(3) Fokwa, B. P. T. Borides: Solid-State Chemistry. In *Encyclopedia of Inorganic and Bioinorganic Chemistry*; Wiley, 2014; pp 1−14.

(4) Akopov, G.; Yeung, M. T.; Kaner, R. B. Rediscovering the Crystal Chemistry of Borides. *Adv. Mater.* **2017**, *29*, No. 1604506.

(5) Boucher, B.; Halet, J.-F.Boron in Solid-State Chemistry: Some Portraits of Metal Borides Taken from a Rich Structural Gallery. In *Handbook Of Boron Science: With Applications In Organometallics, Catalysis, Materials And Medicine*; World Scientific, 2018; Vol. *3*, pp 159−188.

(6) Hosmane, N. S.; Eagling, R.*Handbook Of Boron Science: With Applications In Organometallics, Catalysis, Materials And Medicine*; World Scientific, 2018; Vol. *3*, pp 159−188.

(7) Scheifers, J. P.; Zhang, Y.; Fokwa, B. P. T. Boron: Enabling Exciting Metal-Rich Structures and Magnetic Properties. *Acc. Chem. Res.* **2017**, *50*, 2317−2325.

(8) Halim, J.; Helmer, P.; Palisaitis, J.; et al. Experimental and Theoretical Investigations of Out-of-Plane Ordered Nanolaminate Transition Metal Borides: M_4CrSiB_2 (M = Mo, W, Nb). *Inorg. Chem.* **2023**, *62*, 5341−5347.

(9) Barsoum, M. W. *MAX Phases: Properties of Machinable Ternary Carbides and Nitrides*; John Wiley & Sons, 2013.

(10) VahidMohammadi, A.; Rosen, J.; Gogotsi, Y. The World of Two-Dimensional Carbides and Nitrides (MXenes). *Science* **2021**, *372* (6547), No. eabf1581.

(11) Becher, H. J.; Krogmann, K.; Peisker, E. Über das ternäre Borid Mn_2AlB_2. *Z. Anorg. Allg. Chem.* **1966**, *344*, 140−147.

(12) Ade, M.; Hillebrecht, H. Ternary Borides Cr_2AlB_2, Cr_3AlB_4, and Cr_4AlB_6: The First Members of the Series $(CrB_2)_nCrAl$ with n = 1, 2, 3 and a Unifying Concept for Ternary Borides as MAB-Phases. *Inorg. Chem.* **2015**, *54*, 6122−6135.

(13) Ali, M. M.; Hadi, M. A.; Ahmed, I.; Haider, A. F. M. Y.; Islam, A. K. M. A. Physical Properties of a Novel Boron-Based Ternary Compound Ti_2InB_2. *Mater. Today Commun.* **2020**, *25*, No. 101600.

(14) Nowotny, H.; Dimakopoulou, E.; Kudielka, H. Untersuchungen in den Dreistoffsystemen: Molybdän-Silizium-Bor, Wolfram-Silizium-Bor und in dem System: VSi_2−$TaSi_2$. *Monatsh. Chem.* **1957**, *88*, 180−192.

(15) Ihara, K.; Ito, K.; Tanaka, K.; Yamaguchi, M. Mechanical Properties of Mo5SiB2 Single Crystals. *Mater. Sci. Eng.: A* **2002**, *329*−*331*, 222−227.

(16) Choe, H.; Schneibel, J. H.; Ritchie, R. O. On the Fracture and Fatigue Properties of Mo-Mo3Si-Mo5SiB2 Refractory Intermetallic Alloys at Ambient to Elevated Temperatures (25 to 1300 °C). *Metall. Mater. Trans. A* **2003**, *34*, 225−239.

(17) Fukuma, M.; Kawashima, K.; Akimitsu, J. Superconducting State in (W, Ta)5SiB2. *Phys. Procedia* **2012**, *27*, 48−51.

(18) Aronsson, B.; Lundgren, G.; Hansen, S. E.; Sömme, R.; Stenhagen, E.; Palmstierna, H. X-Ray Investigations on Me-Si-B Systems (Me = Mn, Fe, Co). I. Some Features of the Co-Si-B System at 1000°C. Intermediate Phases in the Co-Si-B and Fe-Si-B Systems. *Acta Chem. Scand.* **1959**, *13*, 433−441.

(19) Li, B.; Duan, Y.; Shen, L.; Peng, M.; Qi, H. Insights of Electronic Structures, Mechanical Properties and Thermal Conductivities of TM5SiB2 (TM = V, Nb, and Ta) MAB Phases. *Philos. Mag.* **2022**, *102*, 1628−1649.

(20) Dahlqvist, M.; Zhou, J.; Persson, I.; et al. Out-Of-Plane Ordered Laminate Borides and Their 2D Ti-Based Derivative from Chemical Exfoliation. *Adv. Mater.* **2021**, 33, No. 2008361.

(21) Tao, Q.; Halim, J.; Palisaitis, J.; et al. Synthesis, Characterization, and Modeling of a Chemically Ordered Quaternary Boride, Mo_4MnSiB_2. *Cryst. Growth Des.* **2023**, *23*, 3258−3263.

(22) Etman, A. S.; Halim, J.; Lind, H.; et al. Computationally Driven Discovery of Quaternary Tantalum-Based MAB-Phases: $Ta_4M''SiB_2$ (M″ = V, Cr, or Mo): Synthesis, Characterization, and Elastic Properties. *Cryst. Growth Des.* **2023**, *23*, 4442−4447.

(23) Werwiński, M.; Kontos, S.; Gunnarsson, K.; et al. Magnetic Properties of Fe_5SiB_2 and Its Alloys with P, S, and Co. *Phys. Rev. B* **2016**, *93*, No. 174412.

(24) Werwiński, M.; Edström, A.; Rusz, J.; et al. Magnetocrystalline Anisotropy of Fe_5PB_2 and Its Alloys with Co and 5d Elements: A Combined First-Principles and Experimental Study. *Phys. Rev. B* **2018**, *98*, No. 214431.

(25) Thakur, J.; Rani, P.; Tomar, M.; Gupta, V.; Saini, H. S.; Kashyap, M. K. In *Tailoring In-Plane Magnetocrystalline Anisotropy of Fe5SiB2 with Cr-Substitution*, AIP Conference Proceeding; AIP Publishing, 2019.

(26) Clulow, R.; Hedlund, D.; Vishina, A.; Svedlindh, P.; Sahlberg, M. Magnetic and Structural Properties of the $Fe_5Si_{1-x}Ge_xB_2$ System. *J. Solid State Chem.* **2022**, *316*, No. 123576.

(27) Rodriguez-Carvajal, J. In *FULLPROF: A Program for Rietveld Refinement and Pattern Matching Analysis*, Satellite Meeting on Powder Diffraction of the XV Congress of the IUCr; IUCr: Toulouse, France, 1990.

(28) Hafner, J. Ab-Initio Simulations of Materials Using VASP: Density-Functional Theory and Beyond. *J. Comput. Chem.* **2008**, *29*, 2044−2078.

(29) Perdew, J. P.; Burke, K.; Ernzerhof, M. Generalized Gradient Approximation Made Simple. *Phys. Rev. Lett.* **1996**, *77*, No. 3865.

(30) Blöchl, P. E. Projector Augmented-Wave Method. *Phys. Rev. B* **1994**, *50*, No. 17953.

(31) Kresse, G.; Furthmüller, J. Efficient Iterative Schemes for Ab Initio Total-Energy Calculations Using a Plane-Wave Basis Set. *Phys. Rev. B* **1996**, *54*, No. 11169.

(32) Monkhorst, H. J.; Pack, J. D. Special Points for Brillouin-Zone Integrations. *Phys. Rev. B* **1976**, *13*, No. 5188.

(33) Wäppling, R.; Ericsson, T.; Häggström, L.; Andersson, Y. Magnetic Properties of Fe_5SiB_2 and Related Compounds. *J. Phys. Colloq.* **1976**, *37*, C6-591−C6-593.

(34) ElMeligy, T. A.; Kota, S.; Natu, V.; et al. Synthesis, Characterization, Properties, First Principles Calculations, and X-ray Photoelectron Spectroscopy of Bulk Mn_5SiB_2 and Fe_5SiB_2 Ternary Borides. *J. Alloys Compd.* **2021**, *888*, No. 161377.

(35) de Almeida, D. M.; Bormio-Nunes, C.; Nunes, C. A.; Coelho, A. A.; Coelho, G. C. Magnetic Characterization of Mn_5SiB_2 and Mn_5Si_3 Phases. *J. Magn. Magn. Mater.* **2009**, *321*, 2578−2581.

(36) Ojiyed, H.; van den Berg, M.; Batashev, I.; Shen, Q.; van Dijk, N.; Brück, E. Magnetocaloric Properties of $Mn_5(Si,P)B_2$ Compounds for Energy Harvesting Applications. *J. Alloys Compd.* **2024**, *978*, No. 173485.